



Geometry of gene regulatory dynamics

David A. Rand^a , Archishman Raju^{b,c}, Meritxell Sáez^{a,d} , Francis Corson^e , and Eric D. Siggia^{c,1}

^aZeeman Institute for Systems Biology and Infectious Epidemiology Research, University of Warwick, Coventry CV4 7AL, United Kingdom; ^bSimons Centre for the Study of Living Machines, National Centre for Biological Sciences, Tata Institute of Fundamental Research, Bangalore 560065, India; ^cCenter for Studies in Physics and Biology, Rockefeller University, New York, NY 10065; ^dThe Francis Crick Institute, London NW1 1AT, United Kingdom; and ^eLaboratoire de Physique de l'Ecole Normale Supérieure, CNRS, École normale supérieure, Université Paris Sciences et Lettres, Sorbonne Université, Université de Paris, 75005 Paris, France

Contributed by Eric D. Siggia, July 28, 2021 (sent for review May 25, 2021); reviewed by Jeremy Gunawardena and Madhav Mani

Embryonic development leads to the reproducible and ordered appearance of complexity from egg to adult. The successive differentiation of different cell types that elaborate this complexity results from the activity of gene networks and was likened by Waddington to a flow through a landscape in which valleys represent alternative fates. Geometric methods allow the formal representation of such landscapes and codify the types of behaviors that result from systems of differential equations. Results from Smale and coworkers imply that systems encompassing gene network models can be represented as potential gradients with a Riemann metric, justifying the Waddington metaphor. Here, we extend this representation to include parameter dependence and enumerate all three-way cellular decisions realizable by tuning at most two parameters, which can be generalized to include spatial coordinates in a tissue. All diagrams of cell states vs. model parameters are thereby enumerated. We unify a number of standard models for spatial pattern formation by expressing them in potential form (i.e., as topographic elevation). Turing systems appear nonpotential, yet in suitable variables the dynamics are low dimensional and potential. A time-independent embedding recovers the original variables. Lateral inhibition is described by a saddle point with many unstable directions. A model for the patterning of the *Drosophila* eye appears as relaxation in a bistable potential. Geometric reasoning provides intuitive dynamic models for development that are well adapted to fit time-lapse data.

Morse–Smale | Waddington landscape | bifurcation | Turing model | gene network

1. Introduction

Much of classical physics, chemistry, and by extension, biology is represented by differential equations. Particularly in biology, the precise form of these equations and their parameters is poorly known. In addition, the long-time behavior of these systems is typically opaque, and one resorts to a case by case numerical solution. Mathematics sidesteps the question of solving a particular equation by using geometric methods to enumerate the discrete types of solutions. Then, qualitative features of the biology may select a type, and mathematics then supplies a minimal parameterization.

A striking aspect of development is the extreme fidelity of the output in response to insults, which nicely aligns with the mathematical notion of genericity (i.e., simply by insisting that all nearby systems are equivalent eliminates exceptional cases that require parameter tuning and are unlikely to be relevant to biology). It is a profound mathematical fact that the assumption of genericity strongly constrains the dynamical behavior. The dynamics appropriate for development are simple; there is a limited number of decisions between different valleys that terminate in discrete cell types. (Chaos or the sensitive dependence to noise is complex mathematically but the antithesis of development.) Expressing a model in geometric language classifies its essential features. In particular, Smale and his school (1, 2) have shown that models that plausibly encompass development all admit a potential that decreases as the system evolves (3, 4). This potential derives from a graph representing which critical

or decision points can flow to which others. Thus, the potential is implicit in, and derived from, the dynamics. Then, the differential equation model can be written as the gradient of that potential times a metric that rescales and reorients that potential. Thus, the Waddington metaphor for development, as flow down a landscape with bifurcations signifying decisions between alternative cell fates, is almost literally true.

Geometric reasoning will typically reduce a genetic model to a few variables per cell, and thus, the explicit connection of variables to genes is lost. However, the typical network for cell communication involves tens of genes; most gene-centric models include only a subset of these and thus, are to some degree phenomenological. Geometry takes this reduction to the extreme and will deliver the minimum number of parameters that cannot be eliminated by variable redefinitions and the minimal phase space for representing the dynamics surrounding a cellular decision.

The results of Smale and colleagues (1–4) do not apply through bifurcation points, which is essential for applications. Thus, we extend their results to encompass bifurcations, both local and global. We limit ourselves to at most three possible states per cell to capture a progenitor cell giving rise to two alternative fates. This is the basic developmental decision, and they can be chained together to describe lineage trees. Within this class, we enumerate all ways the cellular states can be organized by two parameters or morphogens. Our topological arguments yield global results in parameter and state spaces that link together locally described bifurcations.

Geometric methods are well suited to fitting time-lapse data obtained when cells are poised among competing fates. A

Significance

Genetic screens have enumerated the genes that control the process of self-organization that converts a featureless fertilized egg into an embryo. Even the elementary steps may involve 10 genes, so models that attempt to represent each gene contain a plethora of unmeasured parameters. Mathematics has largely categorized the types of solutions that can arise from the equations governing gene networks. These representations are well suited to modern time-lapse imaging, where a limited number of genetic markers are followed in time. Models with minimal parameters that focus on the nonlinear regime from inception to pattern maturation simplify data fitting and provide an intuitive and transparent representation for the dynamics of development.

Author contributions: D.A.R., A.R., M.S., F.C., and E.D.S. designed research, performed research, analyzed data, and wrote the paper.

Reviewers: J.G., Harvard Medical School; and M.M., Northwestern University.

The authors declare no competing interest.

Published under the PNAS license.

¹To whom correspondence may be addressed. Email: siggiae@rockefeller.edu.

This article contains supporting information online at <https://www.pnas.org/lookup/suppl/doi:10.1073/pnas.2109729118/DCSupplemental>.

Published September 13, 2021.

minimal parameterized topographic model with the correct geometry is essential to extract model parameters from the cells as they are transitioning. Merely enumerating terminal fates loses this information. When dealing with many cells, focusing on the bifurcations and saddle points that represent cellular decisions quantifies similarities among all models that use inhibition to define a pattern. Turing showed how chemical reactions plus diffusion can generate patterns in an otherwise uniform system. In geometric terms, the Turing instability is represented as a saddle point, and we show how the trajectory from it to the terminal pattern can be represented by gradient dynamics, thus revealing similarities to models of lateral inhibition by long-range contacts or diffusing factors. Geometric methods are optimal for bridging the time from the initiation of a pattern to its saturation and thus, extracting the essential dynamics of cell specification.

2. The Mathematics of Gene Network Models

A gene network model defines a differential equation that describes the changes on the system with time. The time integration of a differential equation or equivalently, a vector field defines a flow $x \rightarrow \phi^t(x)$, which tells us the state $\phi^t(x)$ at time t if the initial state at time $t=0$ was x . Off points of bifurcation, the rest points p of these systems have well-defined stable and unstable manifolds: that is, (stable manifold) $W^s(p) = \{x | \phi^t(x) \rightarrow p \text{ as } t \rightarrow \infty\}$ and (unstable manifold) $W^u(p) = \{x | \phi^t(x) \rightarrow p \text{ as } t \rightarrow -\infty\}$ (Fig. 1). Moreover, these rest points p are of three types: attractors [$W^s(p)$ empty, they attract all nearby points], saddles [$W^s(p)$ and $W^u(p)$ not empty], and repellors [$W^s(p)$ empty]. We say a saddle has index λ if its unstable manifold has dimension λ .

Two systems have the same qualitative form if there is a homeomorphism sending the trajectories of one onto those of the other. If a system is such that any small smooth perturbation of it does not change its qualitative form, then we say it is structurally stable. In a parameterized family of systems, the parameter values where the qualitative form changes define the bifurcation set. For development, it is natural to focus on systems with a finite number of rest points or periodic orbits. For such systems, a simple set of conditions (1) precisely characterizes structural stability, and these systems are called Morse–Smale (MS) (4).

Periodic behavior is absent in many developmental systems, so we focus on systems without periodic orbits. Also natural for development is our assumption that our phase space M has the topology of the n -dimensional disk and a smooth topologically spherical boundary on which the flow points inward. Consequently, we also do not treat nongeneric bifurcations that take place at the boundary of phase space such as the exchange of stability bifurcation.

The Downhill Structure of Generic Landscapes. The Waddington analogy of development to flow in a topography can be formalized mathematically. All MS systems possess a Liapunov function (a.k.a. potential function) defined on the phase space, which decreases along trajectories and for which rest points (and periodic orbits) are critical points. This formalizes the notion of height in a topography. We call such dynamical systems gradient like. It is commonly thought that this is enough to specify dynamics, but the Liapunov function is not enough to determine where a cell will go when it escapes an attractor (e.g., the potential shown in Fig. 1A is compatible with the dynamical system shown but also with systems where the unstable manifold of the top saddle connects A to C). Therefore, extra information about the dynamics is necessary.

There are two essentially equivalent ways to specify the missing information. One way is to supply the stable and unstable manifolds of the saddle points. The unstable manifolds of the

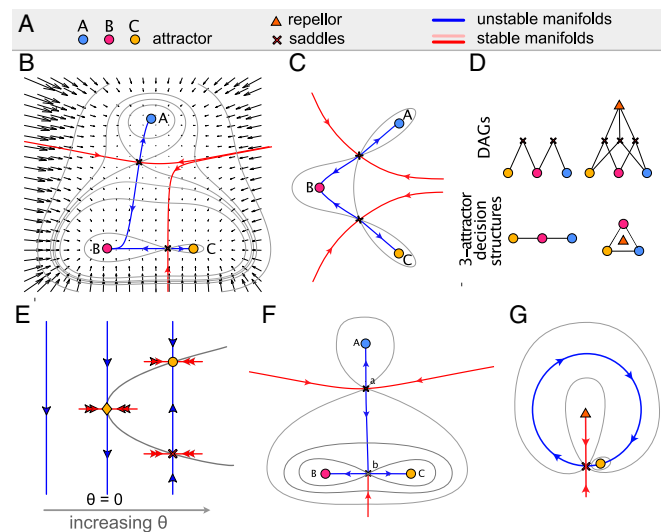


Fig. 1. Representations of MS systems. (A) The symbol set used consistently to describe elements of the phase space or parameter space. (B) An MS system with three attractors and two saddles showing the stable (red) and unstable (blue) manifolds of the saddles. Contours of a potential are shown in gray. In this system, the unstable manifolds meet at the attractor B in a cusp-like shape. (C) In this MS system, which also has three attractors, the unstable manifolds of the saddles make up a smooth curve. (D, Upper) Two examples of DAGs corresponding to the system in B, left side and the CEU of Fig. 5D (B, right side). (D, Lower) The decision structures associated with the DAGs above them. The filled circles represent the attractors, and a connection between attractor A and B means that a cell whose state sits at A (B) can transition to B (A) via a saddle-node bifurcation that destroys A (B). Thus, the connections characterize the escape routes and possible decisions. The connections also correspond to the index 1 saddles in the system that connect A and B. Some escape routes wrap around an index 2 saddle as shown and indicated by a triangle. To minimize the numbers of decision diagrams, we do not distinguish cases where multiple saddles connect the same two fixed points (SI Appendix, section I.7). (E and F) The two simplest bifurcations: the local saddle node and the global heteroclinic flip. These are the main events underlying decision making in our dynamical systems. (E) A saddle-node or fold bifurcation. As θ increases through zero, a saddle and an attractor are born, which then separate with a distance of order $\sqrt{\theta}$. (F) The configuration shown in A can flip to one where the saddle a is connected to C instead of B via a heteroclinic flip. To do this, it passes through the intermediate state shown where there is a heteroclinic connection in which the unstable manifold of the saddle a connects to the saddle at b. (G) An example of a compact landscape involving a repeller. We have taken a case where the attractor is close to the saddle to illustrate that the attractor can move around the circular unstable manifold and collide, undergoing a saddle-node bifurcation and turning the unstable manifold into a limit cycle. This is called an SNIC (Saddle Node on Invariant Cycle) bifurcation. Although it is important to be aware of such bifurcations, we do not consider them anymore since the existence of a limit cycle moves us out of the gradient-like rest point-only systems.

index 1 saddles, for instance, describe the transition routes between attractors.

The other way to augment the Liapunov function is to note that MS systems are nearly gradient systems. In a gradient system, a potential f together with a Riemannian metric g_{ij} completely defines the dynamical system:

$$\dot{x}_i = - \sum_j g^{ij} \frac{\partial f}{\partial x_j}, \quad [1]$$

where $(g^{ij}) = (g_{ij})^{-1}$. The rest points of such a vector field are the critical points of f (g_{ij} is positive definite), and the metric rotates and stretches the potential gradient so it coincides with the vector field. Gradient-like MS systems are also nearly

gradient, and the difference is just at the rest points. By making adjustments of the rest points in arbitrarily small neighborhoods, one can convert the system into a topologically equivalent gradient system (5) (*SI Appendix, section I.A*). The need to adjust the rest points is because at such points, the gradient system has a special structure (e.g., the eigenvalues are real), while the MS system allows complex eigenvalues with nonzero real parts. In applications, the model with its metric abstractly represents how signals distort the landscape and direct cells to the available fates or attractors.

A Directed Acyclic Graph Organizes Cellular Decisions. Now consider an MS system and the graph G whose vertices correspond to the rest points and where two vertices β and β' are connected with a (downward) directional edge (denoted $\beta \succ \beta'$) if there is a trajectory going from β to β' (Fig. 1D). Then, the following nontrivial results hold (6): 1) it is never true that $\beta \succ \beta$; 2) if $\beta \succ \beta'$ and $\beta' \succ \beta''$, then $\beta \succ \beta''$; 3) if $\beta \succ \beta'$, then $\dim W^s(\beta) \leq \dim W^s(\beta')$. Conditions 1 and 2 that exclude $\beta \succ \beta'$ and $\beta' \succ \beta$ are crucial and eliminate heteroclinic cycles (these are not generic). By condition 3, we can naturally attach levels to the nodes of G using the index $d = \dim W^u(\beta)$. The attractors are at the bottom level ($d = 0$), the repellors are at the top, and the index d saddles are at level d . The graph G is a directed acyclic graph, which we shall refer to as the DAG.

Using this, we can allocate heights h_i to the rest points, which for consistency, must satisfy that $h_i > h_j$ whenever $\beta_i \succ \beta_j$, and then, find a Liapunov function h that takes these values at rest points. Moreover, this function can be taken to be a Morse function (2). This means that near each rest point β_i , there is a coordinate system x_1, \dots, x_n such that in these coordinates $h = h_i + \sum_1^n \pm x_j^2$ with the number of minuses equaling the index of β_i .

This height function is unique in the following sense (2). If \hat{h} is another Liapunov function such that the heights $h'_i = \hat{h}(\beta_i)$ are ordered in the same way as those of h , then h and \hat{h} are qualitatively equivalent in the sense that there are homeomorphisms, ϕ of the phase space and ψ of the reals \mathbb{R} , such that $\hat{h}(x) = \psi(h(\phi(x)))$.

As we will see below, a number of advantages flow from these results. Since motion is always downhill, it gives a hierarchical structure to the dynamics and easier understanding of the eventual fates. Second, there is a powerful classification theory for the bifurcations of such systems that is aided by the existence of the potential, and finally, it allows a better understanding of how complexity of such systems can be built up.

Parameterized Landscapes. Our dynamical systems depend upon parameters that will be changed by the signals received by the cell. Changes in the parameters may cause bifurcations where the qualitative nature of the dynamics undergoes a discontinuous change, and these lead to transitions between cell states.

For a given number of attractors or saddles, there are a large number of topologies of landscape potentials. However, if we define a decision as the eventual attractor A reached after the state is freed from its initial attractor B either by a bifurcation destroying B or by stochastically escaping the basin of B , then we can associate with a DAG a unique connected simple graph that we call decision structure (Fig. 1D), which encodes the possible decisions. The number of these is much smaller than the number of landscapes. All three- and four-attractor decision structures are shown in Fig. 1D and *SI Appendix, section I.7*, respectively.

For applications to biology, we consider situations where a precursor cell decides between two alternative fates. Thus, we classify decisions among three or fewer states that depend on two or fewer parameters. The fold bifurcations (Fig. 1E) divide the parameter space up into components in which the

rest points vary smoothly with parameters. We call these MS components. Note that heteroclinic flips can occur within an MS component since rest points change smoothly as you go through the flip.

In what follows, we leverage the continuity of MS dynamics within an MS component to arrive at global representation of the parameter space. The component boundaries consist of smooth fold bifurcation segments that meet in special points that we can enumerate under assumptions of genericity. The sequence of these points around the boundary of the MS component classifies the component. This classification for gradient-like MS systems is global, and it not only tells us what to expect in detailed mechanistic models but also, provides a class of archetypal models that can be parameterized and compared with experimental data (7–9) as described below.

Universality and Normal Forms. It is very useful to contrast our proposed construction of parameterized landscapes with the ideas of a universal unfolding and normal forms that are derived from Thom's theorem (10, 11) that gave rise to catastrophe theory (Fig. 2). This subject assumes strictly gradient dynamics. It then classifies, irrespective of the dimension of state space, the generic local bifurcations in parameterized dynamical systems where the number r of parameters θ (or codimension) is less than five (Fig. 2). By smooth variable changes, any function near the bifurcation can be reduced to a normal form polynomial in one or two dimensions (Fig. 2). The dynamics in the other dimensions are just contraction onto the one or two effective dimensions, thus proving strong dimensional reduction. The parameters in the normal form are the minimum necessary to represent the bifurcation to within variable changes. On the other hand, in parallel with our discussion above about needing to know more than the Liapunov function, it does not classify the global bifurcations in such systems arising from heteroclinic connections (4, 12, 13), which need to be handled separately. Moreover, the results are local in that they only apply close to a bifurcation point.

We aim for results that are global in phase and parameter space and apply to generic parameterized families with a finite number of rest points and no periodic orbits. Nevertheless, the catastrophes of higher codimension are biologically relevant because even if the parameters that we can manipulate to control fates (morphogens) are fewer in number than the codimension, two-dimensional cuts through the full parameter space will occur in our enumeration.

In the following discussion, we focus on generic systems and bifurcations and do not treat nongeneric situations that

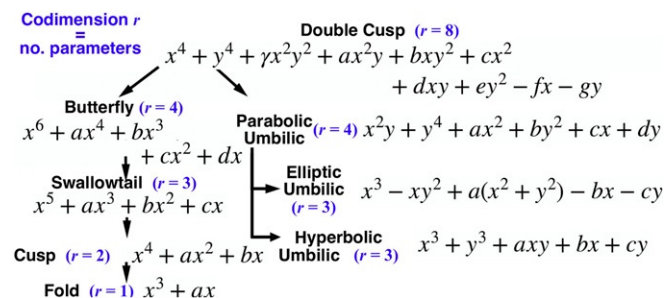


Fig. 2. The hierarchy of elementary catastrophes obtained by coupling two bistable systems. These describe all generic local bifurcations of potentials depending on $r \leq 4$ parameters. If h_θ is such a generic family, then there are coordinates (x_1, \dots, x_n) on phase space such that $h_\theta = f_\theta(y) + \sum_{j=1}^n \epsilon_j x_j^2$ where $f_\theta(y)$ represents one of the elementary catastrophes in the figure, $\rho = 1$ or 2, and the remaining phase space variables can be reduced to a diagonal quadratic form where $\epsilon_j = \pm 1$. Several of these polynomials are prototypes for the parameterized landscapes. A precise statement is in ref. 10.

occur because the system is restricted by, for example, invariant boundaries (e.g., the Lotka–Volterra systems) or symmetries.

Building up Complexity: The Simplest Bifurcations. Any gradient-like MS system can be built up by using just three simple bifurcation types (6). Only two of these are relevant to our

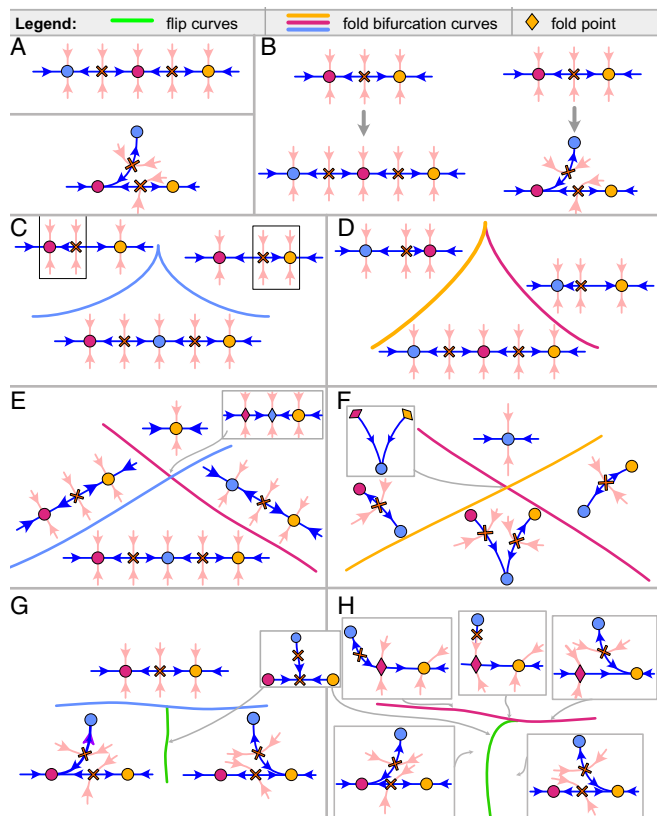


Fig. 3. Building complexity from bistable landscapes using one- and two-dimensional perturbations. The legend is as shown and follows the key in Fig. 1A. (A) We distinguish between these two three-attractor systems, even though they are topologically conjugate, because in applications, the allowed transitions are different. The red attractor cannot undergo a saddle-node bifurcation when the unstable manifolds of the saddles merge in a cusp. The attractors represent biological states that are not equivalent, as they would be under topological conjugacy. (*Upper*) All the rest points lie on a smooth curve defined by the unstable manifolds of the saddles. (*Lower*) The unstable manifolds of the saddles meet at a central sink in a cusp with a common tangency. (B) Fold bifurcations add an extra saddle–sink pair to the bistable system. The new attractor is marked in blue. (C–H) The allowed bifurcation sets for three and fewer fixed points when two parameters are varied. The colored curves denote fold bifurcation curves where the like-colored attractor disappears. (C) Dual cusp. The new attractor in blue, and the saddle is inserted in the middle. For this to occur, the fold bifurcation curve must contain at least one cusp point. (D) Standard cusp. A bistable system has a third attractor added. The cusps in C and D are defined by the discriminant of the same third-order polynomial representing either a source and two saddles or a saddle and two attractors (*cf* Fig. 2). (E and F) Crossing points. Two fold bifurcation curves can intersect transversally, creating a region with a single attractor and a region where there are three attractors. (E) One of the two bifurcation curves involves the central attractor, and then, the attractors must lie on a smooth curve. (F) In this case, the curves correspond to peripheral attractors, and then, both smooth and cusped unstable manifolds are possible. (G and H) There can be a (codimension-2) point on the fold bifurcation curve where the unstable manifold of the top saddle undergoes a heteroclinic flip as shown. Generically, these heteroclinic flips occur on a curve (green). (G) When the source saddle bifurcates away, the flip curve in green intersects the fold bifurcation curve transversely. (H) When the target saddle is destroyed in a fold bifurcation, the flip curve generically terminates in a cusp (*SI Appendix*).

discussion: the fold (Fig. 1E) and the simplest global bifurcation, the heteroclinic flip (Fig. 1F). As we will see, these bifurcations are particularly important for development, and using them provides a powerful method to build complexity that is available for evolution to work on (*SI Appendix, section I.2*).

The fold (a.k.a. the saddle-node) bifurcation results in the appearance of an attracting or repelling rest point and an index 1 saddle as a parameter θ is changed (supercritical case) or the disappearance of the same (subcritical case). More generally, a fold results in the creation/destruction of a pair of saddles of index i and $i+1$. The fold is local in that all the action takes place around a point in parameter and phase space.

When a heteroclinic flip occurs, the unstable manifold of a saddle flips between two different attractors by passing through a state where the unstable manifold of one saddle intersects the stable manifold of the other (i.e., we have a heteroclinic connection) (Fig. 1F).

Fig. 3 shows the generic local ways we can build a system with three attractors starting from a bistable one within a two-dimensional parameter space. Specifically, we show all the ways that folds (codimension-1) defined by a smooth curve in the parameter space can intersect in codimension-2 cusps or crossings (Fig. 3 C–F). Then, Fig. 3 G and H shows the two ways in which a curve of heteroclinic flips can terminate in a fold bifurcation curve, defining a second class of codimension-2 points in parameter space. From these locally described bifurcation sets, we can construct all two-dimensional phase diagrams of MS systems. (Catastrophe theory enumerates higher codimension points, but all the codimension-2 points are contained in our list.)

Dimensional Reduction Characterizes Transitions among Landscapes. Repellers and higher-index saddles can complicate the classification in Fig. 3 (e.g., each index 1 saddle can be replaced by two index 1 saddles and one index 2 saddle). This is handled using the following result (*SI Appendix, section I.A*). As we have seen above, the developmental transitions and decisions are determined by the disposition of the unstable manifolds of the index 1 saddle points relative to the attractors. Thus, a first useful result (*SI Appendix, section I.A*) is that for an MS system in our context one can always find an open set R in n -dimensional phase space that is a decision region in that it contains all the N attractors, all the saddles that connect two attractors, and hence, all nontrivial decision routes. This domain captures almost all trajectories and can be written as the union of open balls R_i containing all N attractors and $N-1$ index 1 saddles where the stable manifolds of the saddles in R_i intersect the boundary ∂R_i , which is a smooth $(n-1)$ sphere transversally in $(n-2)$ spheres (*SI Appendix, Fig. S16*). We call the R_i decision balls. The number needed is less than or equal to the number of index 2 rest points in phase space M . The stable manifolds of the saddles define the boundaries of the basins of attraction for each attractor. Two attractors in adjacent basins are joined by the unstable manifold of the saddle.

As a corollary, for such systems with three attractors, within a decision ball there are two index 1 saddles that connect them, and they have a simple disposition; the unstable manifolds of each saddle each connect to two of the attractors, and they join at one of the attractors (called the central attractor). It is fixed at crossings and cusps (Fig. 3 C–F) but interchanges at flip points. The other attractors are called peripheral. The union of the unstable manifolds is called the connector. At the central attractor, the unstable manifolds join either smoothly or in a nonsmooth fashion. If nonsmooth and this attractor is close to undergoing a fold bifurcation, then the join has a cuspidal shape as in Fig. 3F (*SI Appendix, section I.1*). In either case, the DAG linking the attractors is shown in Fig. 1 D, Left.

The universal dimension-independent topological structure of the attractors, index 1 saddles, and their unstable manifolds that

comes from the existence of the R_i is a statement of dimensional reduction derived purely from the dynamics (*SI Appendix, section I.B*). The restrictions on the configurations of the central attractors that derive from R lead to the results in Fig. 4 and severely constrain the bifurcations that can occur in the boundary of an MS component.

Global Bifurcation Structures. We want to understand the structure of the bifurcations and transitions as the parameters pass into and out of MS components with less than or equal to three attractors and no index 2 rest points. We start by discussing the compact ones Ω (i.e., ones that do not intersect the boundary of the parameter domain). To get the corresponding characterization for noncompact versions, one just opens up the boundary of the MS component, $\partial\Omega$ at a crossing point.

For our discussion, it is necessary to consider the so-called catastrophe manifold (*SI Appendix, section I.3*):

$$\mathcal{M} = \{(x, \theta) | x \text{ is a rest point of } \phi_\theta^t\}.$$

Then, a key point is that, if the parameter space is d -dimensional and the state space is n -dimensional, \mathcal{M} is generically a submanifold of $\mathbb{R}^n \times \mathbb{R}^d$ having the same dimension d as the parameter space (10, 15). Thus, here it is a surface in $n+2$ dimensions. For our systems, the topology of \mathcal{M} is trivial (it is diffeomorphic to a disk) (*SI Appendix, section I.3*), but the way it sits in $\mathbb{R}^n \times \mathbb{R}^d$ and the nontrivial structure of the projection $\chi(x, \theta) \mapsto \theta$ from \mathcal{M} to parameter space are hugely informative.

A point $\mathbf{x} = (x, \theta)$ in \mathcal{M} corresponds to a rest point x of the parameterized landscape at θ , and we will be particularly interested in the subset where x is either a fold or cusp point. Generically, this consists of smooth curves \mathcal{C} (called fold curves), which can either be open and connecting to the boundary of \mathcal{M} or be circles (called fold circles). The part of the bifurcation set

corresponding to folds and cusps consists of the sets $B_C = \chi(\mathcal{C})$ in parameter space, called fold bifurcation curves, where χ is the projection defined above. Although \mathcal{C} is smooth, B_C will typically have cusp points as in Figs. 3 and 5. A smooth piece of a fold bifurcation curve is called a fold bifurcation segment. If \mathcal{C} is a fold circle, then B_C is a closed curve without self-intersections (*SI Appendix, section I.3*).

Now, a key result that will lead to our characterization of MS components is the following. If $\mathbf{x} = (x, \theta) \in \mathcal{M}$ is on a fold curve \mathcal{C} , then through x there is a center manifold (4), and as \mathbf{x} moves along \mathcal{C} , the tangent $\ell(\mathbf{x})$ to this center manifold varies in a smooth fashion. At x , the time evolution determines a definite positive direction and orientation on $\ell(\mathbf{x})$ (Fig. 4B). Generically, as \mathbf{x} moves along a fold curve \mathcal{C} , this orientation flips only at cusps, and so, counting orientation flips gives the number of cusps in \mathcal{C} (*SI Appendix, section I.4*).

From this observation, we readily get all the results in Fig. 4, and these provide tight constraints on what can happen in the boundary of a three-attractor MS component (Ω in parameter space) as we now explain. By definition, the attractors vary smoothly in Ω with the parameters and maintain their identity.

As one proceeds around $\partial\Omega$, there is a sequence of codimension-2 points $\theta_1 \dots \theta_N$ with $\theta_N = \theta_1$ as described in Fig. 3, namely cusps, dual cusps, crossings, and the two types of endpoints of flip curves. If we know these, then we know the bifurcation structures associated with Ω and $\partial\Omega$. The points θ_i and θ_{i+1} are joined by a smooth fold bifurcation segment ℓ_i . The bifurcations on this segment involve one of the attractors X_i , and we say that the attractor identity of ℓ_i is X_i .

Fig. 5 contains the simplest MS components that involve all three attractors and are not decomposable into two attractor systems. Fig. 5A is the minimal system with a dual cusp (*SI Appendix, section I.5*). In this case, if the parameters are inside

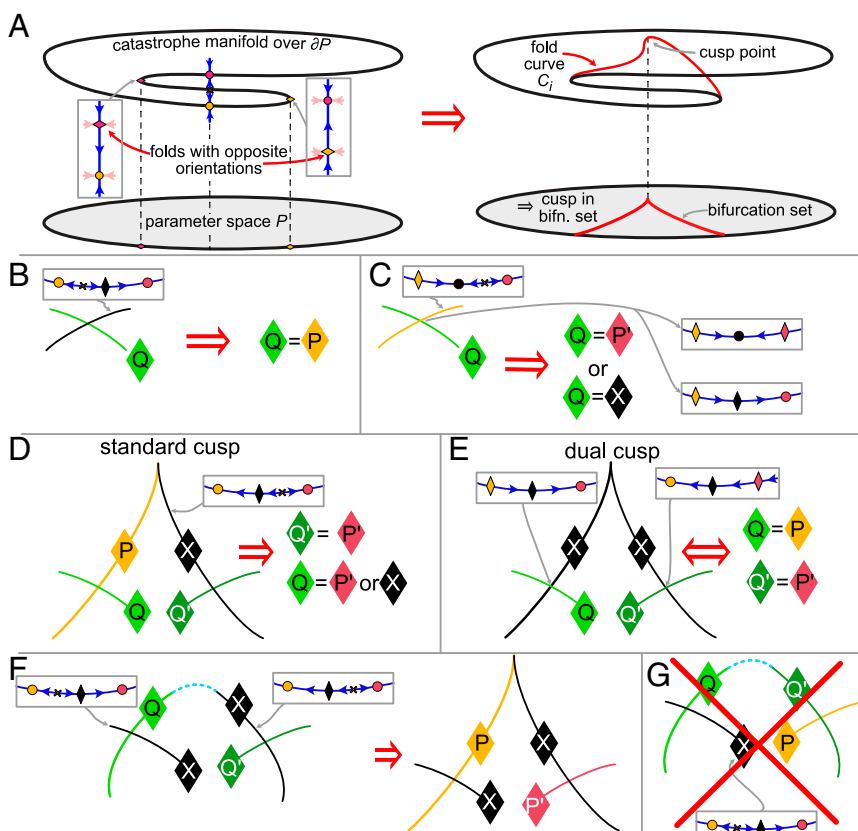


Fig. 4. The legend is the same as in Figs. 1A and 3. (A) Over part of the boundary ∂P of a two-dimensional domain of parameter space P , we assume we have an S-shaped bistable section and that the system is monostable over the rest of ∂P . Then, it follows that under very mild conditions (*SI Appendix, section I.4E*) inside P , there must be at least one cusp (ref. 14 has $n=1$ case). This is because there must be a fold curve joining the two folds shown, and on this fold curve, the two folds shown have opposite orientations. (B–G) Local rules governing the disposition of cusps and crossings in the boundary of a three-attractor MS component. X is always the central attractor, P, P' peripheral. (B) The orientation of the fold bifurcation involving the central attractor determines the possible transverse crossings of the fold bifurcation curve. On the black fold bifurcation curve, the central attractor bifurcates with the saddle to its right (connected to red); thus, the only allowed crossing is the bifurcation of the yellow attractor with its saddle. (C) The peripheral attractor involved in the fold constrains the possible crossings of the fold bifurcation curve. (D) Standard cusp. Fold bifurcation curves crossing the cusp's branches satisfy the conditions in B and C. (E) Dual cusp. Fold bifurcation curves crossing the cusp's branches satisfy the conditions in B and C, and the crossings imply the existence of the cusp. (F) The opposite orientations of the folds of the central attractor on the two fold bifurcation curves as shown imply the existence of a cusp. (G) If $Q - Q'$ is a single-fold bifurcation curve, certain consecutive crossings are not possible. By B, $Q = P$, but P cannot intersect itself; so, if $Q' = X$, then the next intersection can only be with P' via D.

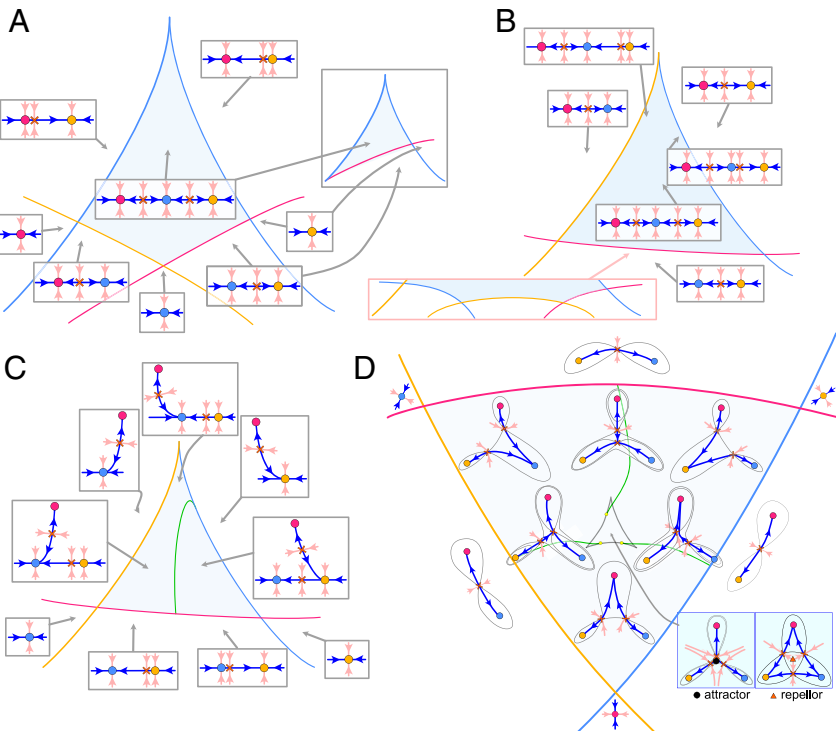


Fig. 5. Minimal three-attractor MS components (light blue). The legend is the same as in Figs. 1A or 3. The color of a fold bifurcation curve indicates the attractor that bifurcates on it. (A) The minimal MS components containing a dual cusp. Inset shows the minimal system involving a dual and standard cusp. The MS components with less than or equal to two attractors are a subset of this for the dual-cusp case. (B) Minimal MS component for a standard cusp. Inset in the pink box shows a simple alternative configuration replacing the red curve at the bottom of the cusp. (C) The same for a standard cusp and a flip curve. Note that for parameters near a cusp point, the connector among the three attractors will be smooth. The intersection of the flip curve (green) is cusped when it hits the fold for the central attractor and transverse when the peripheral (red) attractor disappears. There is a second curve emanating from the cusp in the flip curve where the connector changes from smooth to cusped. (D) The CEU. Inside the MS component boundary and outside the triangular hypocycloid B_C , there are three attractors and two saddles. This dynamical system can be obtained by taking the gradient dynamical system of the potential associated with the potential $f_\theta(x, y) = x^4 + y^4 + x^3 - 2xy^2 + a(x^2 + y^2) + \theta_1x + \theta_2y$, with respect to a generic Riemannian metric. The term $x^4 + y^4$ is added to the usual polynomial for Thom's elliptic umbilic in order to make the dynamical system compact. It has the effect of adding the three attractors and the outer fold bifurcation curves to the three saddles. The sign of the parameter a controls whether the central rest point is an attractor or repeller. By the MS inequalities (6), this is a minimal effect.

Ω and the state starts in the central attractor (blue), then it stays there unless the parameters cross the curves through the cusp. Then, it transitions to either peripheral attractor depending upon the branch crossed. For this reason, we regard this as an all-or-nothing landscape because a population of cells with their initial state at the central attractor would all transition to the same new state upon bifurcation. An intimately related minimal MS component is shown in Fig. 5A, *Insets*. This involves a dual and a standard cusp joined together.

The simplest MS components containing a standard cusp are those in Fig. 5B and C. The difference between them is the existence of the flip curve (green) shown in Fig. 5C. The transitions allowed using the landscape in Fig. 5B are rather limited. If parameters start in Ω , one can only transition to or from one of the peripheral attractors and cannot transition to the other one.

The transitions are richer with the flip curve as it enables bifurcations that can change the central attractor and the escape routes available to cells. On this curve, there is a heteroclinic connection from the saddle connected to the red peripheral attractor (the source) to the other saddle (the target). The flip curve joins tangentially to the side of the cusp where the central attractor (blue) and target saddle disappear in a fold. The flip curve must either terminate on the same fold bifurcation segment or end on the fold bifurcation curve where the source saddle and red peripheral attractor disappear as in Fig. 5C. If one considers populations of cells in each of the three attractors, then on the boundaries of Ω , transitions out of red are possible and between blue and yellow but not into red. This landscape illustrates a downhill flexible choice. Near the lower red fold bifurcation curve, a signal that repositioned the flip curve would control the fractions that populated the other two attractors (*SI Appendix*, section I.5).

More complex structures involving combinations of these cusps and more crossing points are possible, but these also are highly

constrained as described in *SI Appendix*. These more complex versions are unlikely to occur in experiment since morphogens are apt to act monotonically on cell fates, and the new complexity is just multiple appearances of the same fold bifurcation.

Finally, we need to consider the case where there are no cusps in the MS component boundary $\partial\Omega$; then, only crossing points are involved. The case of two crossing points is trivial and is decomposable in the sense that it is a two-attractor MS component with a nonbifurcating attractor added. However, the case of three crossing points is already extremely interesting.

This gives the configuration shown in Fig. 5D with three smooth fold bifurcation curves corresponding to each of the attractors. The simplest example with such an MS component boundary is what we call the compactified elliptic umbilic (CEU) (Fig. 5D), and one can show that any three-attractor MS component with such a boundary consisting of smooth fold bifurcation curves is just a more complex version of the CEU. It automatically has nontrivial monodromy because if one traces around a simple closed curve γ just inside of this boundary, the two saddles are interchanged. Together with an analysis of the curves of heteroclinic connections that must occur, this implies that γ contains a bifurcation curve Ω_C where C is a fold circle containing an odd number of cusps in three groups corresponding to the three cusps in the CEU (*SI Appendix*, section I.6).

We emphasize that these results follow from the properties of a gradient-like MS system; we do not assume a gradient system.

Note that biology takes place around \mathcal{M} . Thus, in the vicinity of the cusp in Figs. 4A and 5B, it is possible to find a path in parameter space along which a population of cells in one attractor transitions smoothly to a second attractor without crossing a fold bifurcation curve. Thus, although one is crossing a fold point in parameter space, if there are no cells at the attractor that disappears, it is invisible in an experiment.

3. Illustrative Examples

A good illustration of how the prototype categories in Fig. 5 can be used to fit single cells differentiating in response to time-dependent morphogens is the paper by Sáez et al. (9) using mouse stem cells. The first of two transitions was a dual cusp (Fig. 5A) that depending on a morphogen, deposited the pluripotent cells into either an anterior neural or caudal epiblast state that cannot interconvert. The second transition entailed a flip bifurcation to flexibly allocate cells to one of two attractors, corresponding to part of Fig. 5D. This shows how data can distinguish the global flip bifurcation from the local saddle node and how three-way decisions can be chained together into a decision tree.

Another example of a dual cusp was found in a model for the mouse blastocyst that places a weakly stable inner cell mass state between the primitive endoderm and epiblast (ref. 16, SI appendix, figure S4). The development of the vulva in *Caenorhabditis elegans* is a clear example of three cell fates and an elliptic umbillic (7). It was also fit by the authors of ref. 8 as an instance of Fig. 5C.

The examples that follow show how the theory extends to spatial pattern formation with an emphasis on the decision points. In section 3A, we present a kinetic model involving Hill functions with an elliptic umbillic parameter space that applies equally well to three cells that are on/off. This should make more tangible the abstract (Fig. 5). The information carried by the metric is examined in section 3B. In section 3C, we show how long-range inhibition is equivalent to a decision structure with a cascade of progressively more stable saddle points and suggest how the Riemannian metric is constructed around the various rest points. For the Turing model in section 3D, we show how the dynamics on the unstable manifold from the initial instability to the final pattern can be fit by a simple but universal potential formulation. Finally, in section 3E, we show that patterning behind a wave simplifies when expressed in potential form.

A. The Three-State System Has an Elliptic-Umbillic Parameter Space. The discussion surrounding Fig. 5 envisioned multiple states for one cell. However, the examples would apply equally well to a model of three interacting cells each with a single binary state with mutual repression among the active forms. The mathematics is agnostic to the biological interpretation (Fig. 6). We chose to work around a point in parameter space with permutation symmetry in the three cells to simplify the parameter search, but the result persists so long as the three boundary curves have the topology shown (Fig. 5D).

B. A Flow Defines a Potential. Consider a typical two-variable activator-inhibitor system, $\dot{a} = f_a(a, h) - \nu a$, $\dot{h} = f_h(a) - h$, which is ubiquitous in signaling pathways. They pose an

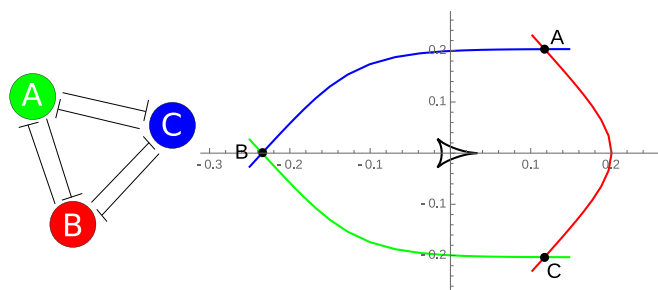


Fig. 6. A symmetric three-cell or gene network with mutual repulsion and the elliptic umbillic conformation (Fig. 5D). The outer colored lines are the fold curves when one of the states disappears (three attractors become two). At the points A, B, and C, there is one stable rest point and four with eigenvalues $\sim (-1, 0, -1)$ (i.e., the intersection of two fold lines). The inner black contour consists of three fold lines, and inside, it is an index 2 saddle, three index 1 saddles, and three attractors.

ostensible challenge to represent in potential form since we have $\partial_a f_h > 0$, the activator turns on h ; while $\partial_h f_a < 0$, the inhibitor represses a . Thus, the cross-derivatives have opposite signs, so it is of interest to reduce these to potential form. The system has two stable fixed points and a saddle. While there is a general construction for the potential in any MS system (17), for purposes of illustration we show a more intuitive construction in two dimensions by defining the potential as the integral of the vector field along the trajectory to the stable fixed points and then making the two functions smooth across the stable manifold of the saddle (Fig. 7). The inverse metric, g^{ij} , is defined as the sum of two projection operators, one that projects the potential streamlines along the direction of the flow and one that projects it in a direction tangent to the contour (SI Appendix, section II.2). Together, they define a proper metric that aligns the potential gradient to the flow, except near the rest points where a separate construction is necessary and the two pieces are then glued together.

C. Patterning by Lateral Inhibition. Inhibition is ubiquitous in biology and is manifest on the epidermis of many animals as a sparse array of hairs, feathers, or sensory bristles. How are these patterns established? A recent model for sensory bristle patterns in a fly (19) nicely illustrates what is plausibly an MS system with a hierarchy of rest points organized into the DAG of Fig. 1D and the process of gluing local potential representations around critical points to model the complete system.

Each cell i is described by a single variable $0 \leq a_i \leq 1$ where the value 1 corresponds to the neural fate that will develop into a bristle. In the terminal state, the bristles are spaced by four to five cell diameters in all directions. Cells are initialized with $a_i \sim 0$ and are confined to a strip by inhibition from the surroundings so that the initial pattern formation is one-dimensional along the strip and then extends laterally. We generalize Fig. 6, three cells that mutually inhibit, to a periodic ring of N cells with long-range inhibition represented as

$$\begin{aligned}\dot{a}_i &= \sigma(a_i - h_i) - a_i, \\ h_i &= \sum_{j \neq i} K_{i,j} d(a_j),\end{aligned}\quad [2]$$

where $\sigma(a)$ and $d(a)$ are sigmoidal functions of their arguments varying between zero and one. The kernel $K_{i,j}$ is a Gaussian function of the distance between cells i, j , so the sum h_i is the net inhibition seen by cell i .

The qualitative behavior of the model can be understood from Fig. 8A. When $h < 0.37$, only $a = 1$ is stable, while for $h > 0.63$, only $a = 0$ is stable, with bistability in between. Initially $h = 0$, all the a_i values grow from zero, and cells inhibit their neighbors with the result that trajectories peel off from a common envelope. Which cells turn on is a sensitive function of initial conditions and noise, but the kernel will keep neural precursor cells well separated.

The first “decision” is defined by the principal saddle point on the diagonal $a_i = a$, where a varies from ~ 0.9 for $N = 2$ cells to ~ 0.51 for N large. At this point, the number of unstable directions scales $\sim N$. For $N = 8$ in Fig. 8B, the Jacobian matrix is symmetric and there are five unstable nearly identical eigenvalues and three stable eigenvalues. Proceeding down the DAG from the most unstable saddle, we find a state $\sim (1, 1, 1, 0, 1, 1, 1, 0)$ that has four unstable directions, as does a second less symmetric state with only cells 4, 7 off and the others on to varying degrees. States with fewer unstable directions and various patterns of on/off cells can all be found. Thus, for very physical reasons this model generates a rich DAG. There are also stable terminal states that are not reflection invariant

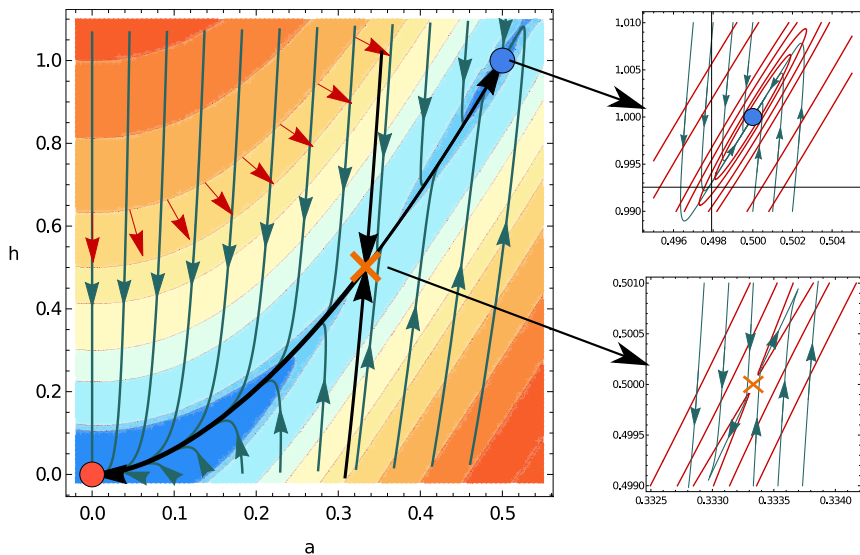


Fig. 7. A potential constructed for a prototype activator-inhibitor system with flows shown in green. Contours of the potential, which is defined as the integral of the vector field along the trajectory to the stable fixed point, are shown going from low (blue) to high (red) potential. The red arrows on one of the contour lines show the flow from the gradient of the potential. Since the equations have a nonzero curl, a metric is required to align the red and green arrows. The construction does not work near the fixed points, but a separate potential and metric can be defined there (18) and glued to the global potential (details are in *SI Appendix*, section II.2). (Insets) Plots of the contour lines in red and flow magnified near the upper fixed point and the saddle are also shown.

on the circle such as $\sim(1, 0, 0, 1, 0, 0, 0, 0)$, but these were not found as the endpoint of the dynamics when initializing with small randomized a_i .

To reproduce the flow around the principle saddle point on the diagonal from a potential, we propose what is essentially an antiferromagnet but with a diagonal inverse metric (n.b. $d(a)$ in Eq. 3 is identical to Eq. 2):

$$\dot{a}_i = -g(a_i)\nabla_{a_i}F, \\ F = \sum_i V(a_i) + \frac{1}{2} \sum_{i \neq j} d(a_i)K_{i,j}d(a_j). \quad [3]$$

In *SI Appendix*, section II.3, we show that we can match both the location of the principle saddle point on the diagonal, $a_i = \bar{a}(N)$, and the Jacobian for any number of cells N by fixing two functions of a single variable, g and V . The solution for g near the origin behaves as $g(a) \sim a$ in contrast to Eq. 2, where the velocity is $\mathcal{O}(1)$ (compare Fig. 8B with Fig. 9). However, since the saddle point is restricted to $a > 0.51$, we can easily correct the inverse metric for smaller a .

The dynamics derived from these potential models are shown in Fig. 9, where it is obvious comparing with Fig. 8B that we have corrected the dynamics around the origin with the two-part inverse metric, at the expense of now making the decrease of single a_i in response to the antiferromagnetic repulsion too abrupt. However, that can plausibly be fixed by adjusting the metric in a separate region of the phase space.

Putting the original model in potential form shows the extent to which the entire pattern formation process is controlled by

the saddle point on the diagonal. Analytic calculations for how small differences amplify are facilitated by knowing the stable and unstable manifolds of the saddle.

We started from a very idealized model, but if it were elaborated to include a more realistic description of the Notch-Delta signaling that is responsible for the inhibition or a more complete account of the neural fate, we suspect that the principal saddle point will retain its unstable directions but add many more stable ones. The best estimate for how much those additional details disappear from the dynamics is in fact the stable eigenvalues at the saddle point.

One may object that any model with contact inhibition is unrealistic since signals have to travel diffusively. That point is somewhat debated in *Drosophila* after cellularization (20, 21), but nevertheless, we show in the next section, when diffusion is responsible for communication between cells, that the underlying potential models have the structure discussed here. Finally, representing a biological decision as a saddle point in a high-dimensional space applies during mesoscopic times, from when the pattern first emerges to when it is close to saturation.

D. The Turing Model in Potential Form. A Turing system is an activator inhibitor pair a, h where the inhibitor diffuses much more rapidly than the activator. We want to capture the unstable manifold leading from linear instability of the uniform system to the localized patch of activator and ignore the slow rearrangements of the pattern after the activator saturates. Thus, it suffices to consider Turing systems on a circle with parameters that give a single localized state, modulo symmetries.

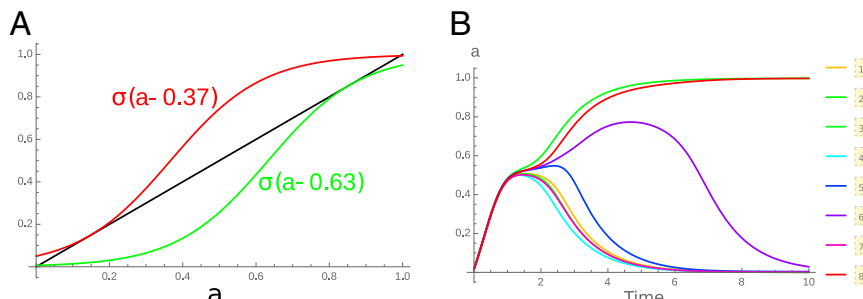


Fig. 8. Behavior of Eq. 2. (A) Values of inhibition h for which the \dot{a} equation has saddle-node bifurcations. When h from neighboring cells is < 0.37 , only the $a = 1$ state is stable, bistability persists for $0.37 < h < 0.63$, and only the $a = 0$ state exists for larger h . The diagonal is shown in black. (B) Eight cells on the circle with a kernel chosen to allow only two cells with $a = 1$ at the end. The time to reach steady state can vary by $2 \times$ depending on whether a third cell hangs close to the saddle point as seen here vs. Fig. 9.

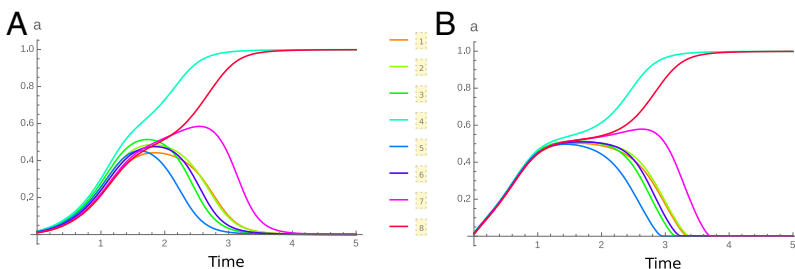


Fig. 9. Two potential models for Eq. 2 run with the same initial conditions. (A) The potential in Eq. 3 with the inverse metric extending to the origin. (B) The inverse metric near the origin now matches Eq. 2.

We add diffusion to the system in section 3B:

$$\begin{aligned}\dot{a}(x, t) &= f_a(a, h) - \nu a + D_a \partial_x^2 a, \\ \dot{h}(x, t) &= f_h(a) - h + D_h \partial_x^2 h.\end{aligned}\quad [4]$$

A straightforward reduction of Eq. 4 around the saddle point to potential form would require the Laplace operator in the inverse metric (*SI Appendix, section II.4*), which is not useful. A much more informative representation is derived by starting from a discrete version of Eq. 4.

When linearized around the uniform state, there will be $2N$ modes that generally occur in pairs when reflection symmetry connects two inequivalent states that vary in space (i.e., with cell index i). Due to the large value of D_h/D_a , there will be $N - 1$ very stable modes centered on the h_i and one modestly stable one for uniform h . In the a sector of the spectrum, the uniform mode is stable by the definition of a Turing system (the first unstable mode is nonuniform and defines the scale of the terminal pattern), and among the remaining, a few will be positive in pairs. The most stable eigenvalue for both a and h may be a singleton or in a pair depending on whether N is even or odd.

Fig. 10 shows the case of $N = 7$ with one unstable pair of modes. The dynamics can be projected on the (linear) tangent space of the unstable modes at the saddle point. The unstable manifold is sevenfold symmetric, compact, and flat enough that its projection onto the tangent space is 1:1. At the boundary of the unstable manifold, there are seven fixed points, related by rotational symmetry, and between them, seven saddles each with one unstable direction (Fig. 10).

The dynamics on the tangent plane can be accurately parameterized in polar coordinates relative to the central saddle by the system

$$\begin{aligned}\dot{r} &= \lambda r - \beta r^3, \\ \dot{\theta} &= g(r) \sin(7(\theta - \theta_0)),\end{aligned}\quad [5]$$

where $g(r)$ is a Gaussian tightly centered at $\sqrt{\lambda/\beta}$, the system is $2\pi/7$ periodic, and θ_0 is a phase shift. The equations in [5] are potential with $g(r)$ acting as an inverse metric. However, the precise form of $g(r)$ is not crucial since as N increases, the number of fixed points increases accordingly, and the angle dependence disappears, leaving an invariant circle on which the radial motion terminates.

We have reduced the dynamics from the $2N$ dimensions to the two dimensions of Fig. 10, with a rate parameter λ and a limiting radius. All the complexity of $f_{a,h}$ in Eq. 4 is reduced to these two numbers and manifestly could not be made any simpler. This describes the entire unstable manifold from the linear instability to the finite amplitude stable state. Still missing is the embedding of the radius variable r in the tangent space into the physical fields a, h that we will deal with after properly treating the continuous case. However, this embedding is by definition time independent, all the dynamics live in r , and we thus have a very compact representation of a time-dependent field

with accuracy at the few percent level, more than adequate for biology.

Guided by the discrete case, we represent the continuum equations around the saddle point as a linear term that we can Fourier transform on the circle and a nonlinear term local in position that we expand to third order. Our restriction to mesoscopic times makes it entirely reasonable to work on a compact space. Call the most unstable Fourier mode k_1 , and if we close the system with cubic nonlinearity within this space, we must obtain an equation of the form $\dot{z}_1 = \lambda_1 z_1 + f_3 z_1 |z_1|^2$, where z_1 is the complex coefficient of that Fourier mode. If a second unstable mode $|k_2| = 2|k_1|$ exists, then we find couplings between the modes as in

$$\begin{aligned}\dot{z}_1 &= \lambda_1 z_1 - \beta z_1 (|z_1|^2 + 2|z_2|^2) - 2\gamma z_1^* z_2, \\ \dot{z}_2 &= \lambda_2 z_2 - \beta z_2 (|z_2|^2 + 2|z_1|^2) - \gamma z_1^*.\end{aligned}\quad [6]$$

The k_2 mode describes two incipient blobs on the circle that under our assumptions, are unstable to a single blob (i.e., the k_1 mode grows faster). The unstable manifold is now four-dimensional and goes to a fixed point through a series of saddle points, each with one less unstable mode. The first and second of these saddles correspond to a state with two blobs and these saddles are inaccessible for typical initial conditions. Thus, we have described the dynamics of the cross-over between two blobs and one on the circle with four modes and dynamics derived from a potential. One consequence of these equations is that the angles of the two modes are locked as shown in Fig. 11. We

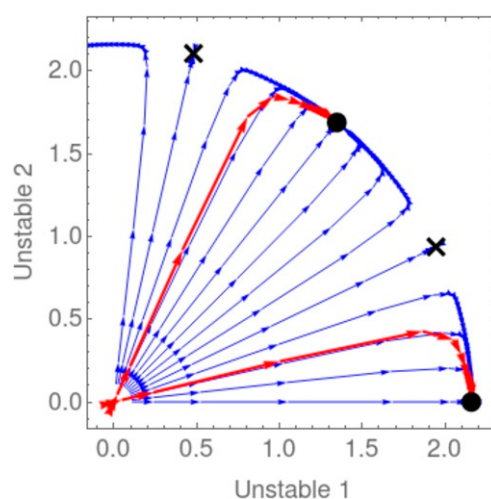


Fig. 10. A sector of the tangent plane to the unstable manifold at the saddle for a discrete version of Eq. 4 with $N = 7$ cells. The blue arrows show the trajectories of the potential fit with different initial conditions chosen at equally spaced angles. The red arrows show the projection of the actual equations on the tangent plane. Arrows are plotted at equal times and so, give the approximate velocity.

note that the model is potential with trivial metric only to cubic order, and higher-order Taylor series would induce a nontrivial metric.

To map the modes $z_{1,2}$ back to the continuum a, h , we have to interpolate between the Fourier modes for the linear system and the static solution for a , which is a single blob. The simplest way to model this constraint is to simply add the Fourier modes linearly and saturate them with a sigmoidal function $\sigma(x)$ at medium and late times, reflecting the high and low values of a . Thus, one needs to fit the parameters in Eq. 6 as well as the sigmoidal function shape as a function of z_1 and z_2 to map our potential to continuum a . The comparison is plotted in Fig. 11C, with details in *SI Appendix*, section II.4.

To illustrate the utility of this reduced representation for fitting experimental data, consider a two-dimensional continuum periodic rectangular system, which leads to the formation of three blobs. Each of these blobs is slightly different because of a long-range gradient as well as randomness in the microscopic equations. However, our reduced representation captures the essential nature of the dynamics, and the different blobs can be fit with different parameters in the radial mode in Eq. 5 as shown in Fig. 12.

When presented with time-lapse data for a Turing system, we would take the radial profile of each blob as a function of time and fit to a single time-independent sigmoidal function composed of a solution to r in Eq. 5, with parameters and initial conditions specific to each blob. We expect that this procedure will collapse considerable variability among the dynamics of the blobs to universal functions with minimal parameters as in Fig. 12.

We conclude this section by generalizing the lateral inhibition model (Eq. 2) to one with a diffusing inhibitor, which is instruc-

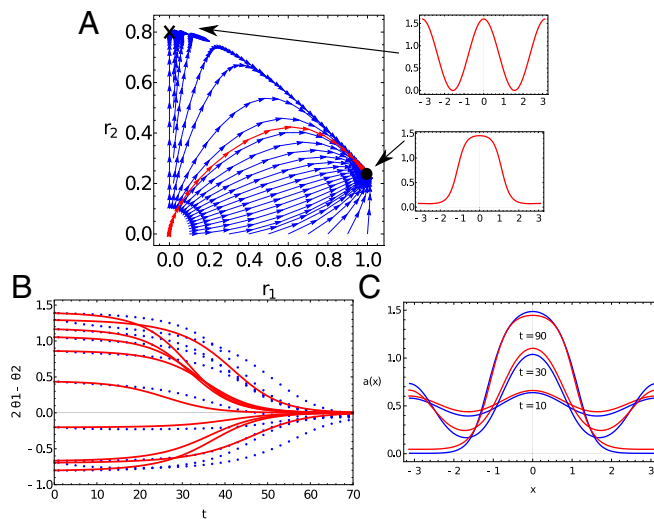


Fig. 11. The continuous Turing PDE (Partial Differential Equation) is solved and projected onto the variables z_1 and z_2 in Eq. 6 by simply doing a linear projection onto the Fourier modes ($z_i = r_i e^{i\theta_i}$). (A) The streamlines of Eq. 6 in the space of the two radii with the angles set to zero showing a two-dimensional projection of the four-dimensional unstable manifold. The callouts show the terminal profiles of $a(x)$ at the saddle with two peaks and the fixed point with one. The initial condition is $a(x) = 0.01 \cos(2x) + 0.001 \cos(x)$. (B) Eq. 6 implies that the angles stably lock together with $2\theta_1 - \theta_2 = 0$. This is shown with blue dots for the actual Turing model and red for the potential fit for various initial conditions. (C) A saturation function is required to match the solution in the tangent space in (a, h) to $a(x)$ in physical space x . The solution of the continuous system (blue) is compared with a sigmoidal saturation of the tangent space flow (red) for the red cross-over trajectory in A.

tive to compare with the Turing system. Consider the system for N cells periodically continued (suppressing constants):

$$\begin{aligned}\dot{a}_i &= f_a(a_i) - h_i d'(a_i), \\ \dot{h}_i &= d(a_i) - h_i + D_h(h_{i+1} + h_{i-1} - 2h_i),\end{aligned}\quad [7]$$

where $d(a)$ is again a sigmoidal function mapping a into the interval $[0, 1]$. There is no loss of generality in making the coupling between h and a in \dot{a}_i the derivative of the source of h in \dot{h}_i since we can redefine a to make this true. For illustration, we assume $f_a(a) \sim a$ around the origin to make that point unstable. If we solve $\dot{h}_i = 0$ for h_i and substitute into the \dot{a}_i equation, we obtain the contact (rapid diffusion) form of the equations with the Greens function appropriate to the circle (i.e., Eq. 3). The cross-derivatives $\partial_h \dot{a}$ and $\partial_a \dot{h}$ are equal and opposite in sign as we expect for inhibition.

For an example with all constants order one and the D_h adjusted to produce the desired spacing between the active cells, there is again a saddle point along the diagonal with $\sim N$ stable directions corresponding to the h_i and a few additional ones with weight in the a_i directions. A few of the stable eigenvalues can be complex, reflecting the nonzero antisymmetric terms in the Jacobian matrix. The unstable eigenvalues are numerically very close to those of the system with h_i eliminated, and the dynamics within the a_i subspace are identical for practical purposes (*SI Appendix*).

So, in comparison with the Turing system, there are now many unstable modes all deriving from the same saddle point along the diagonal in a_i . The origin is unstable rather than stable, and the dynamic competition that generates the pattern derives from the saddle point on the diagonal. We believe that the geometric viewpoint provides the clearest characterization of these two systems with diffusing inhibitors.

E. Spreading the Pattern by a Wave. When a two-dimensional area is to be patterned, the process often proceeds from a boundary, which provides the template. One such system is the morphogenic furrow in the fly eye. It moves as a wave from posterior to anterior across the eye imaginal disk, leaving behind the hexagonal crystal of ommatidia that characterizes the insect eye (22).

We follow the ideas of ref. 23, which modeled this system with effectively three modes: a cell-localized activator a , an intermediate-range inhibitor that is responsible for the spacing between successive rows of ommatidia, and a long-range activator b that destabilizes the $a = 0$ state ahead of the furrow to allow the cells to compete as described in Eq. 7. We will replace the dynamic inhibitor in our reformulation with static lateral inhibition, which we just showed to be functionally equivalent.

We can directly formulate our model as a potential since there is no sign conflict when integrating two activators. We thus propose in one dimension

$$\begin{aligned}u(a, b) &= v(a) + (b - a^2)^2/2 - ab, \\ U &= \sum_{i=1}^N u(a_i, b_i) + D_b(b_i - b_{i-1})^2/2 + \frac{1}{2} \sum_{i \neq j} d(a_i) K_{i,j} d(a_j),\end{aligned}\quad [8]$$

where constants are omitted, $v(a)$ is a bistable potential, and the double sum copies Eq. 2. The boundary conditions are open, and we fix $b_0 = 1$ so that the left end of the lattice is activated and the wave propagates toward $i = N$. The only condition on the one-cell potential $u(a, b)$ is that the origin $a, b = 0$ is stable and the saddle point occurs around $a, b \sim 0.1$ in units where the final state shows $a \sim 1$ in the active cells, 0 elsewhere, and $b \sim 1$ (the value of the saddle point is small but not tiny and stabilizes the

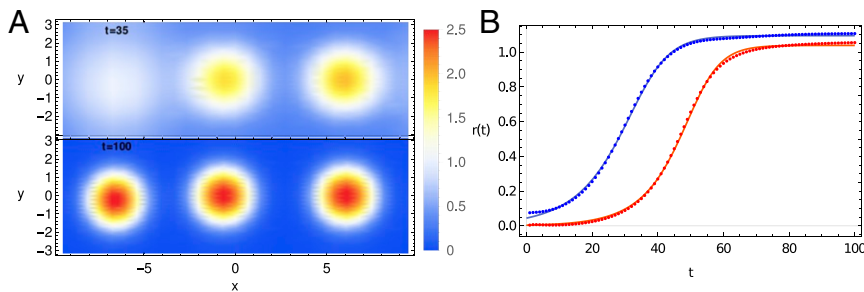


Fig. 12. (A) A model in two spatial dimensions leads to the formation of three blobs, each of which are slightly different because of randomness in the parameters and initial conditions. The blobs are shown at two different time points, demonstrating that the left and right ends form at different times. Since the blobs have spherical symmetry, the profile is first averaged over angles and then projected onto the Bessel function $J_0(R)$ being the first term in a Fourier–Bessel series, where R is a scaled radial coordinate in space. (B) The simulated two-dimensional dynamics are projected onto the tangent plane (dots) for the left (red) and right (blue) blobs in A. The data are fit very well by the radial part of Eq. 5 (curve) with parameters specific to each blob. The space–time profiles in A are then fit by a sigmoid depending on $r(t)$ from Eq. 5 and $J_0(R)$ (*SI Appendix, section II.4*).

cells at $a = 0$ until the leading edge of the wave of b arrives by diffusion and kicks them over the saddle). The static inhibition controls the spacing between the active cells, and the diffusion constant governs the speed within limits (Fig. 13).

The potential formulation makes it obvious that the moving solution in Fig. 13 is just an instance of relaxational dynamics for a field with two minima, the simplest instance being $f_x(sa - a^2/2 + a^4/4 + D(\partial_x a)^2/2)$, $s \ll 1$ where an interface between locally stable solutions at $a \sim \pm 1$ moves to replace the higher potential solution with the lower potential one and does so with constant velocity.

F. A Static Morphogen Gradient and Adaptive Systems. We note in closing two instances where the components are few enough in number and well-enough characterized that gene-centric models are informative and quantitative, yet the geometric viewpoint poses questions that are often neglected (*SI Appendix*).

A morphogen is a diffusible factor whose level defines cell fate. Morphogen systems, like any other dynamical model, may be multistable, implying hysteresis in the pattern. An informative geometrical representation is given in *SI Appendix, section II.6*.

An adaptive system has one variable that responds to an external signal yet whose value is signal independent under static conditions. Adaptation is common in biology from sensory systems to signaling pathways, where it is a more rapid way to

connect position to fate than reading a static signal (24). This property is succinctly expressed in the form of a potential and metric (*SI Appendix, section II.7*).

4. Discussion

We have given a tight argument that in the absence of periodic behavior, robust (i.e., structurally stable) gene regulatory dynamics satisfy the MS assumptions and thus, can be described by a downhill gradient-like system where the rest points can be organized into a DAG defining the allowed transitions between them. Moreover, we observed that such dynamics can reasonably be represented as a true gradient system given by a potential and a Riemannian metric. The mathematics achieves such sweeping results by imposing genericity; system properties are unchanged in a neighborhood of the system in question. In analogy, embryonic development is robust against environmental noise.

In geometric terms, the inhibition among cells that produces a sparse array of neural progenitors is simply a high-index saddle point that initiates the DAG. A cascade of saddle points followed with decreasing index to the terminal pattern. Turing pattern formation begins from the linear instability of a uniform state, making it a saddle point. Its nonlinear development is just the unstable manifold of the saddle that we represented as an MS system.

A representation of the flow as a metric and potential continues to work around saddle-node bifurcations and heteroclinic flips, the two operations needed to grow any MS system from the trivial one (6). These operations are thus the only topology changing “mutations” that are needed to computationally evolve gene regulatory networks (25).

The results of catastrophe theory are clearly of relevance to our analysis, but they are local; since they only study the potential, they do not capture the stable and unstable manifolds of the dynamics or the heteroclinic flips. Our study shows that the latter are crucial to understanding developmental dynamics, and the study of them opens up ways to extend the theory from local to global.

In particular, we borrowed from the mathematics that Smale developed for his proof of the high-dimensional Poincaré conjecture to rigorously deduce a form of dimensional reduction in which for generic systems like ours, the topological relationship between index 1 saddles and attractors is effectively independent of dimension and can be represented by two-dimensional systems. The canalization of Waddington is simply the focusing of the dynamics onto the unstable manifolds of the saddles. The results in Fig. 5 depend upon this understanding, which is very different from the dimension reduction that catastrophe theory supplies that only applies locally in state and parameter space.

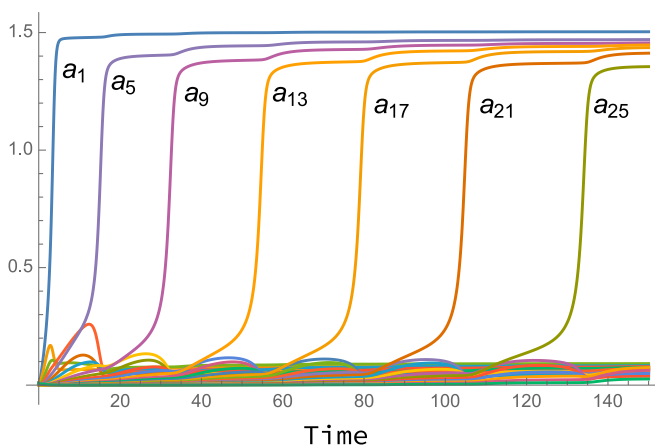


Fig. 13. Dynamics for the one-dimensional morphogenetic furrow from Eq. 8 for $n = 30$, where every fourth cell is active. The wave appears to slow toward the end since the long-range activator b is diffusing out the right-hand boundary. For the same reason, the plateau in a_i is a bit lower at the end. Solutions with periods 2 to 5 all have energies below the initial state, but only period 4 appears behind the wave.

A network model represented by activating and inhibitory arrows among genes has little relation to the geometry of the flow: that is, the ultimate representation of the dynamics. We expect that such models with two parameters and less than or equal to three attractors will produce the bifurcation diagrams in Fig. 5.

Recent examples of modeling development have taken a more geometric approach from the start. We already mentioned in section 3 (9), where the authors fit the first few steps of differentiation of stem cell in response to various morphogens. In ref. 26, the so-called triple points in the phase diagram of the *C. elegans* vulva plausibly correspond to Fig. 5D, and a related study (8) used Fig. 5C. If embryonic stem cells can transition directly to ectoderm, mesoderm, and endoderm, then Fig. 5D is a possible model with the pluripotent state being the fourth attractor in the center.

Cartoons of development commonly represent the succession of fates as a binary tree, suggesting the existence of three attractor systems at the nodes. Left implicit is a developmental clock that biases fate progression in one direction. This could be a competence window that limits the response to signals to a temporal interval combined with epigenetic changes.

There is no reason that our analysis cannot be generalized to periodic systems where the structurally stable dynamics are also MS. All the key ingredients regarding MS systems are available (with obvious changes such as a constant potential on the periodic orbit) (2), but the generic bifurcations are more numerous and complex, which makes this a substantially more challenging task. When a developmental system is subject to an autonomous periodic signal, such as might be the case with the cell cycle, the relevant dynamics are represented by a map rather than by a flow as we have assumed so far, and this opens up a richer corpus of behavior.

In applications, the states in question are rarely terminal; thus, parameters are not static. When systems are not steady, do all the other degrees of freedom have time to relax to the two dimensions necessary to represent all three-way decisions? This question can only be resolved by fitting data, and in examples, we have seen that high-index saddles can also have multiple stable

directions, which is then the recipe for quantifying the neglected variables.

The geometric description is compact since all reference to specific genes is lost, yet experiments commonly mutate genes and observe changes in patterning dynamics and outcomes. Clearly, each mutant requires at least one parameter to fit, but is there any way to predict a double mutant from each of the single ones? An interesting ansatz was used in ref. 7, where a single-vector sigmoid function was wrapped around the non-compact polynomial equations for the dynamics. A linear force added to the sigmoid rendered the dynamics bounded, but the dependence on the two morphogens was entirely linear inside of the sigmoid. The double mutant was thus the sum of the single ones. Nevertheless, the model captured the essential genetic interactions. While the qualitative details of the problem dictate the geometry, how it is parameterized is very germane for applications.

We have concerned ourselves exclusively with representing gene networks as potentials but not with morphogenesis for which forces and potentials are natural. Morphogenesis and fate assignment are tightly coupled in development as exemplified by the ordered expression of the HOX genes during the unfolding of the anterior-posterior axis (27), but it is as yet unclear how to unify potentials for fates and forces.

Data Availability. All study data are included in the article and/or *SI Appendix*.

ACKNOWLEDGMENTS. We thank James Briscoe, John Guckenheimer, and David Lubensky for discussions. D.A.R. thanks Ian Stewart for very helpful early discussions. D.A.R. and M.S. were funded for this work by Engineering and Physical Sciences Research Council Grant EP/P019811/1. D.A.R., F.C., and E.D.S. participated in the 2019 Kavili Institute Program on quantitative biology supported by NSF Grant PHY-1748958, NIH Grant R25GM067110, and Gordon and Betty Moore Foundation Grant 2919.02. A.R. acknowledges support from the Simons Foundation. M.S. was supported by the Francis Crick Institute, which receives its core funding from Cancer Research UK, the UK Medical Research Council, and Wellcome Trust (all under Grant FC001051). F.C. was supported by the Agence Nationale de la Recherche Grant ANR16-CE13-0003-02. E.D.S. was supported by NSF Grant 2013131.

1. S. Smale, On gradient dynamical systems. *Ann. Math.* **74**, 199–206 (1961).
2. K. R. Meyer, Energy functions for Morse-Smale systems. *Am. J. Math.* **90**, 1031–1040 (1968).
3. S. Smale, Differentiable dynamical systems. *Bull. Am. Math. Soc.* **73**, 747–817 (1967).
4. J. Guckenheimer, P. Holmes, *Nonlinear Oscillations, Dynamical Systems, and Bifurcations of Vector Fields* (Springer Science & Business Media, 2013), vol. 42.
5. S. Newhouse, M. Peixoto, There is a simple arc joining any two Morse-Smale flows. *Asterisque* **31**, 15–41 (1976).
6. S. Smale, “Morse inequalities for a dynamical system” in *The Collected Papers of Stephen Smale*, F. Cucker, R. Wong, Eds. (World Scientific, 2000), vol. 2, pp. 596–602.
7. F. Corson, E. D. Siggia, Geometry, epistasis, and developmental patterning. *Proc. Natl. Acad. Sci. U.S.A.* **109**, 5568–5575 (2012).
8. E. Camacho-Aguilar, A. Warmflash, D. A. Rand, Quantifying cell transitions in *C. elegans* with data-fitted landscape models. *PLoS Comput. Biol.* **17**, e1009034 (2021).
9. M. Sáez et al., A quantitative landscape of cell fate transitions identifies principles of cellular decision-making. *bioRxiv* [Preprint] (2021). <https://www.biorxiv.org/content/10.1101/2021.03.11.434982v1> (Accessed 11 March 2021).
10. C. Zeeman, “The classification of elementary catastrophes of codimension ≤ 5 ” in *Structural Stability, the Theory of Catastrophes, and Applications in the Sciences*, P. Hilton, Ed. (Springer, 1976), pp. 263–327.
11. R. Thom, Topological models in biology. *Topology* **8**, 313–335 (1969).
12. J. Guckenheimer, *Bifurcation and Catastrophe in Dynamical Systems* (Elsevier, 1973), pp. 95–109.
13. B. A. Khesin, Bifurcations in gradient dynamic systems. *J. Soviet Math.* **52**, 3279–3305 (1990).
14. I. N. Stewart, Catastrophe theory and equations of state: Conditions for a butterfly singularity. *Math. Proc. Camb. Philos. Soc.* **88**, 429–449 (1980).
15. V. I. Arnold, V. Afrajmovich, Y. S. Il'yashenko, L. Shil'nikov, *Dynamical Systems V: Bifurcation Theory and Catastrophe Theory* (Springer Science & Business Media, 2013), vol. 5.
16. L. De Mot et al., Cell fate specification based on tristability in the inner cell mass of mouse blastocysts. *Biophys. J.* **110**, 710–722 (2016).
17. Z. Nitecki, M. Shub, Filtrations, decompositions, and explosions. *Am. J. Math.* **97**, 1029–1047 (1975).
18. A. Bosch, The factorization of a square matrix into two symmetric matrices. *Am. Math. Mon.* **93**, 462–464 (1986).
19. F. Corson, L. Couturier, H. Rouault, K. Mazouni, F. Schweisguth, Self-organized Notch dynamics generate stereotyped sensory organ patterns in *Drosophila*. *Science* **356**, eaai7407 (2017).
20. C. Alexandre, A. Baena-Lopez, J. P. Vincent, Patterning and growth control by membrane-tethered Wingless. *Nature* **505**, 180–185 (2014).
21. T. B. Kornberg, Scripting a place in time. *Dev. Biol.* **447**, 24–27 (2019).
22. N. E. Baker, Patterning signals and proliferation in *Drosophila* imaginal discs. *Curr. Opin. Genet. Dev.* **17**, 287–293 (2007).
23. D. K. Lubensky, M. W. Pennington, B. I. Shraiman, N. E. Baker, A dynamical model of ommatidial crystal formation. *Proc. Natl. Acad. Sci. U.S.A.* **108**, 11145–11150 (2011).
24. B. Sorre, A. Warmflash, A. H. Brivanlou, E. D. Siggia, Encoding of temporal signals by the TGF- β pathway and implications for embryonic patterning. *Dev. Cell* **30**, 334–342 (2014).
25. P. François, Evolving phenotypic networks in silico. *Semin. Cell Dev. Biol.* **35**, 90–97 (2014).
26. F. Corson, E. D. Siggia, Gene-free methodology for cell fate dynamics during development. *eLife* **6**, e30743 (2017).
27. T. Iimura, O. Pourquié, Hox genes in time and space during vertebrate body formation. *Dev. Growth Differ.* **49**, 265–275 (2007).